

# 1 Mechanical analyses of flat sheet water treatment membranes

2 Murat Ozdemir <sup>1</sup>, Selda Oterkus <sup>1,\*</sup>, Erkan Oterkus <sup>1</sup>, Islam Amin <sup>1,2</sup>, Abdel-Hameed  
3 El-Aassar <sup>3</sup> and Hosam Shawky <sup>3</sup>

4 <sup>1</sup> PeriDynamics Research Centre, Department of Naval Architecture, Ocean and Marine  
5 Engineering, University of Strathclyde, 100 Montrose Street, Glasgow G4 0LZ, UK

6 <sup>2</sup> Department of Naval Architecture and Marine Engineering, Port Said University, Port Said 42511,  
7 Egypt

8 <sup>3</sup> Egypt Desalination Research Centre of Excellence (EDRC) and Hydrogeochemistry Department,  
9 Desert Research Centre, Cairo 11753, Egypt

10 \* **Correspondence:** selda.oterkus@strath.ac.uk; Tel: +44-141-548-4979.

11 **Abstract:** In this work, we address the mechanical response of the flat sheet polymeric water  
12 treatment membranes under the assumed operational loading conditions. Firstly, we perform  
13 quasi-static analyses of the membranes under normal pressure loads, which is the condition that  
14 resembles the actual loading for flat sheet membranes in the submerged membrane bioreactors. Then,  
15 the long-term deformation of the membranes is studied under the assumed filtration durations for the  
16 same loading conditions by utilizing the viscoelastic material models. The quasi-static and  
17 viscoelastic membrane simulations are performed by a commercial finite element code ANSYS.  
18 Finally, the mechanical fatigue life predictions are carried out based on the stress distributions from  
19 the quasi-static analyses and the long-term effects from the viscoelastic analyses.

20 **Keywords:** mechanical analysis; flat sheet; water treatment; membrane; fatigue; viscoelasticity  
21

---

## 22 1. Introduction

23 As the consequences of the climate change have been more evident in the recent decade, it is  
24 crucial to utilize the water resources effectively. These impacts are more severe for the societies in  
25 geographically disadvantageous parts of the earth. In this regard, reuse of wastewater plays a  
26 prominent role in a sustainable water management. Among the water reuse applications, membrane  
27 bioreactors have a significant place [1]. Both organic and inorganic based materials can be adopted  
28 as the membrane materials; however, the organic based polymeric membranes are relatively popular  
29 thanks to their lower investment costs [2]. On the other hand, the polymeric membranes are  
30 vulnerable to mechanical degradation caused by harsh content of the feed water, backwashing as well  
31 as the chemical cleaning [3].

32 The structural integrity of the membranes holds a substantial importance for a reliable water  
33 filtration operation and so the public health and environmental considerations. Wang et al. [4]  
34 presented an extensive literature study, which covers useful techniques for the evaluation of  
35 mechanical characterization of membrane materials. Among them, the first method that comes to  
36 mind is the uniaxial tensile tests for the strength and stiffness evaluation of membrane materials. The

37 parameters that can be obtained by the uniaxial tensile tests are: stress–strain curves, Young's  
38 modulus, yield stress, ultimate stress and elongation at break [4]. Ahmed et al. [5] studied the  
39 mechanical strength of (PVDF-HFP) composite flat sheet membranes for efficient oil-water  
40 separation process using standard dog-bone specimens. The uniaxial tests can also be employed for  
41 hollow fibre type membranes made up of either organic [6] or inorganic based materials [7].  
42 Dynamic Mechanical Analysis (DMA) is another suitable technique to characterize the viscous  
43 behaviour of polymeric materials under various environmental conditions [8]. Viscous damping  
44 properties of the membranes can be determined by DMA under various temperature and test  
45 frequencies [9]. Though the uniaxial tensile tests for the mechanical response characterization of the  
46 membranes are relatively generic, the actual loading condition and the response of flat-sheet  
47 membranes can be resembled by the bursting tests [4]. Lalia et al. [10] investigated the mechanical  
48 properties of PVDF-HFP flat sheet membranes using the bursting tests.

49 To the best of authors' knowledge, the mechanical fatigue life prediction of water treatment  
50 membranes under filtration cycles has not been reported yet. This issue has also been reported in the  
51 review work of Wang et al. [4]. One of the similar works that can also be employed for the water  
52 treatment membrane was presented by Mackin et al. [11], which investigates the mechanical fatigue  
53 life of polymeric films under biaxial stress state using a spherical indenter. Their experimental work  
54 was supported by the finite element (FE) analyses as well as the nonlinear membrane theory in [11].

55 Taking into account the lack of works on the fatigue life predictions of water treatment  
56 membranes in the open literature, we aim to present a general framework on the mechanical response  
57 analysis of flat-sheet water treatment membranes under realistic operational pressure loads. The main  
58 focus is given to fatigue life prediction; however, the viscoelastic creep deformation and its impact  
59 on the membrane performance are also to be addressed in the present work.

60 The outline of the present manuscript is established as follows. Section 2 is dedicated to  
61 description of case studies, evaluation of membrane material properties as well as the problem setup.  
62 The quasi-static analysis by Finite Element Method (FEM) are performed for filtration and  
63 backwashing pressure loads in Section 3.1. The viscoelastic analyses for the long term deformation  
64 prediction of the membranes under filtration are performed in Section 3.2. The stress and strain  
65 values obtained from the quasi-static and viscoelastic FE analyses are utilized for fatigue life  
66 predictions in Section 3.3. Finally, Section 4 presents the concluding remarks.

## 67 2. Materials and Methods

68 In the membrane bioreactors, the flat-sheet membranes are compacted in cassette form, which  
69 includes the frames and spacers. The frame is the component that provides the structural integrity of  
70 the membrane module under filtration and backwashing pressure loads, while the spacers are utilised  
71 to lead permeate flow inside the membrane cassette for the hydrodynamic efficiency [12]. Apart  
72 from the hydrodynamic impact of the spacers, flat-sheet membranes are supported by the spacers  
73 especially under the filtration process. During the backwashing, the spacers will not have any  
74 structural support unless special arrangements are considered for membranes, see [13].

75 The membrane sheets with spacers are schematically illustrated in Figure 1. In the given figure,  
76 the cassette frame is not demonstrated for simplicity. The spacers are assumed to be fixed to cassette  
77 frame at the ends, so are the membrane sheets. The spacers also prevent the contact of the  
78 membranes with each other.

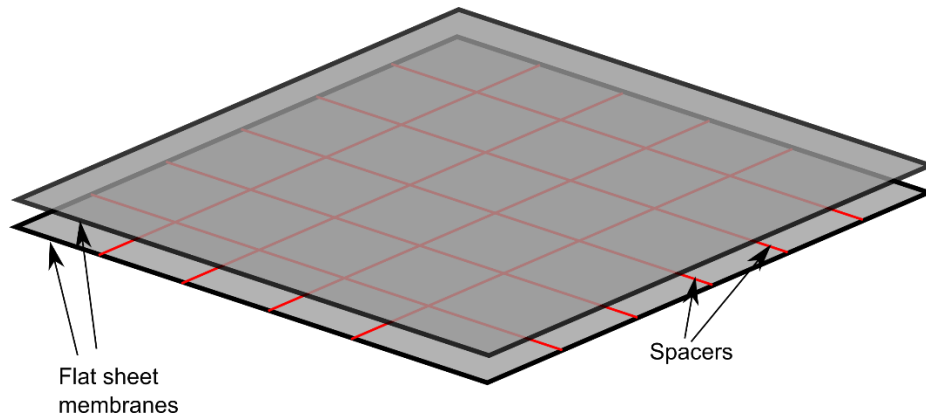


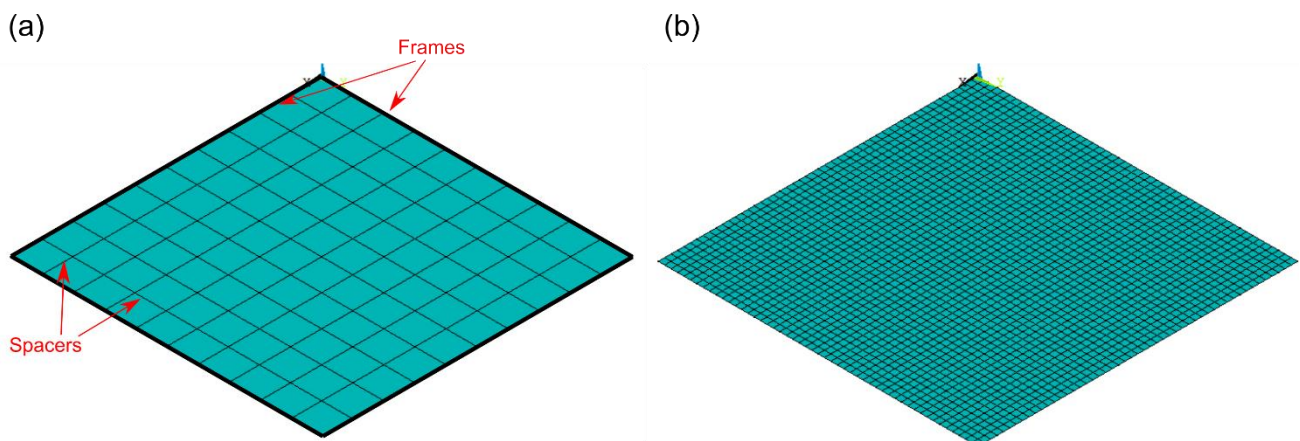
**Figure 1.** Flat sheet membrane model with spacers.

79  
80  
81

## 82 2.1. FE Modeling

83 The membrane sheets are subjected to hydrostatic pressure in the submerged configuration;  
84 however, the driving force for the filtration is usually generated by the vacuum pressure on the  
85 permeate side of the bioreactor. Then, we will assume that the both sheets will be subjected to same  
86 pressure due to the main vacuum condition on the permeate side. The influence of the hydrostatic  
87 pressure change on the total pressure load can be omitted.

88 The vacuum pressure ideally sucks the membranes towards each other, and the contact of the  
89 membrane sheets is prevented by the spacers. This sucking condition is represented by the normal  
90 pressure on the membrane surfaces in the FE models. Moreover, the FE model can be simplified by  
91 modelling only one sheet with suitable boundary conditions (BCs). The representative model of the  
92 membrane and associated FE mesh are shown in Figure 2.



93

94 **Figure 2.** Simplified membrane modelling: (a) Representative membrane sheet model with  
95 spacers and framing, (b) FE mesh model of the membrane sheet.

96 We will consider two different spacer configurations, which divide the membrane sheets into 10  
97  $\times$  10 and 20  $\times$  20 sub-regions. The spacer configurations have been selected for illustrative  
98 purposes and they may have significant effect on the mechanical response. It is expected that the  
99 spacers will support the membrane sheet under the filtration pressure. It is also noted that the design

drive for the spacer configurations is usually the hydrodynamic performance [12]. The procedure, which shall be presented next is ideally applicable for any spacer configuration for the flat sheet membranes. Figure 2 (a) demonstrates the case with the  $10 \times 10$  sub-regions. The principal dimensions of the membrane sheet will be kept same throughout the study, and they are assumed as  $L \times W \times t_m = 500 \times 500 \times 2$  mm regardless of the spacer configuration. Here, the parameters stand for the length, width and thickness of the membrane sheet, respectively. The thickness of the membrane has been decided so that the membrane can withstand high pressure values with relative coarse spacer configurations ( $10 \times 10$  configuration); however, the procedure in the present work is applicable for any thickness of flat-sheet membranes.

### 2.1.1. Loading and BCs

As described in the preceding section, the load is applied as normal pressure on the membrane surfaces for both filtration and backwashing operation. In the implementation of the BCs, we make some assumptions that reflect the realistic condition with sufficient simplicity. The membrane's edges along the framing lines are assumed to be fixed, i.e., both translations and rotations of the membrane sheet are constrained along the edges.

The spacers are invoked in the FE models in a simplified manner to avoid computational burden and the possible numerical instabilities arising from multiple contact points, which might be the case if the spacer and membrane sheets are modelled separately and the contact conditions are introduced. So, the spacers are not modelled explicitly, but suitable BCs are introduced along the spacer lines as shown in Figure 2 (a). The boundary conditions for the spacers under filtration condition are as follows.

(i) The displacement component normal to the membrane surface is constrained.

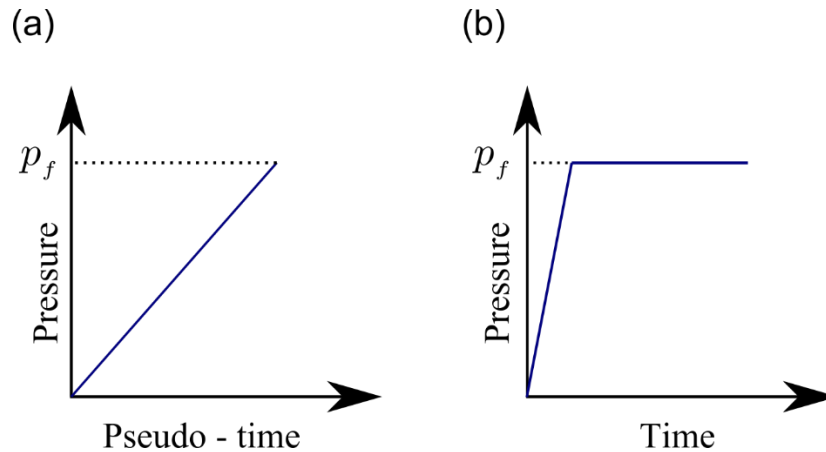
(ii) The rotation component about the axis parallel to the spacer line is constrained.

The latter condition is a reasonable assumption since the suction condition will create non-rotation region along the spacer lines under the real operation. On the other hand, if the backwashing is employed, the membrane sheet is supposed to deform outwards, and the spacers will have no support against membrane deformation. It is therefore assumed that the membrane sheets will deform freely under backwashing, and the BCs for spacers mentioned above are not applicable for the backwashing condition.

The load implementation is to be set regarding the requirements for a stable FE solution for both quasi-static and viscoelastic simulations. In the case of quasi-static analyses, the desired pressure load, either for filtration or backwashing case, is increased gradually until the desired value is attained. If the viscoelastic analysis is the case, the load has to be implemented and should be kept constant for a desired duration. In the FE framework, the viscoelastic analysis is essentially transient analysis without inertia effects.

In the transient analysis, the load can be applied in two ways: (i) ramped loading, (ii) stepped loading [14]. Stepped loading is ideal for the viscoelastic analysis since we aim to keep the load constant for a certain duration; however, the sudden implementation of loading may cause numerical difficulties because of the excessive deformation in some elements. In this regard, the pressure load is gradually increased until the desired pressure level in a relatively short amount of time, then the load magnitude is kept constant. The load implementation schemes for quasi-static and viscoelastic analyses are illustrated in Figure 3. In this figure, the time parameter in the quasi-static analyses is

142 not the physical time and this is the reason for the term “Pseudo-time” in Figure 3 (a).



143

144 **Figure 3.** Load implementation schemes for: (a) Quasi-static analyses, (b) Viscoelastic  
145 analyses.

#### 146 2.1.2. FE mesh and element properties

147 In the modelling of membrane sheets, we employ Shell181 elements in ANSYS package. Since  
148 we aim to perform viscoelastic analysis in addition to accurate stress results from a series of  
149 quasi-static analyses, full integration option of the stiffness matrix is adopted.

150 Mesh density is adjusted based on the spacer configuration. If the membrane sheet is divided  
151 into  $10 \times 10$  sub-regions by the spacers, the number of elements between the spacer lines  
152 (boundary of sub-regions) is set as five. As for the cases with  $20 \times 20$  sub-regions, the number of  
153 elements between the spacer lines is set as three. The domain discretization for backwashing  
154 conditions is performed in the same manner so as to keep the number of nodes/elements consistent.  
155 Figure 2 (b) shows the density of FE mesh for the  $10 \times 10$  sub-regions case.

#### 156 2.1.3. Evaluation of the material properties

157 The material properties are derived from the work of Emori et al. [15]. The reference work  
158 performs both experiments and FE calculations regarding the creep behaviour of the hollow fibre  
159 membranes involving 3D pore geometry. In the present work, we will assume that our membrane  
160 sheets are fabricated by the same material tested in [15].

161 The generic material properties are adopted from the tensile tests provided by [15]. The  
162 experimental stress-strain curve for the highest strain rate, i.e.,  $\dot{\epsilon} = 1.4 \times 10^{-2}$  in [15], is digitized;  
163 then the Young's modulus and yield stress are derived from the digitized curve as  $E = 138.9$  MPa  
164 and  $\sigma_Y = 4.04$  MPa. With a reasonable approach, the approximate yield strain for the membrane  
165 material is calculated as  $\epsilon_Y = 0.029$ . FE quasi-static analyses are performed by employing these  
166 material properties.

##### 167 2.1.3.1. Viscoelastic properties

168 As far as the viscoelastic simulation is concerned, the time dependent material properties have to

169 be introduced. In ANSYS FE code, the viscoelastic material properties can be represented by  
 170 generalized Maxwell model comprised of Maxwell elements and a spring element, which are  
 171 connected parallel to each other [16]. The relaxation of the viscoelastic material is mathematically  
 172 represented by the Prony series, which have the exponential decay terms. The viscoelastic material  
 173 properties are ideally provided by the relaxation of the shear modulus as expressed below by a Prony  
 174 series expression.

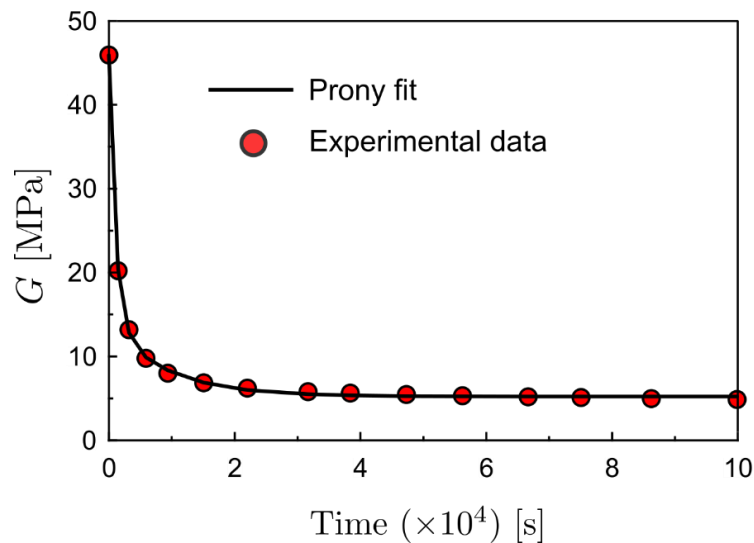
$$175 \quad G(t) = G_\infty + \sum_{i=1}^{N_M} G_i \times e^{(-t/\tau_i)} \quad (1)$$

176 In Eq. (1),  $G_\infty$  denotes the shear modulus of the material when the time converges to infinity,  
 177 which basically represents the elastic stiffness of the single spring element on the generalized  
 178 Maxwell model.  $G_i$  is shear modulus of each Maxwell element, while the relaxation time of each  
 179 Maxwell element is represented by  $\tau_i$ . The number of Maxwell elements in the model is defined as  
 180  $N_M$ .

181 For the PVDF material tested in [15], the fundamental material properties are given previously in  
 182 this section. The same material was tested under constant loads to capture the creep deformation in  
 183 the same work [15]. We will take the results of the creep tests presented in the reference work to  
 184 obtain the viscoelastic material properties. Here, it must be noted that the applied load at the creep  
 185 tests should be below the elastic limits so that we can assume the membrane deformation comprises  
 186 elastic and viscous parts but the plastic deformation does not occur. In this regard, we have chosen  
 187 the creep test result for 3 N axial loading in Ref. [15]. This axial load corresponds to approximately  
 188 3.6 MPa axial stress, which is below the yielding point, and is sufficiently large to provide valuable  
 189 creep data. Once the data provided for 3N in Figure 4 of Ref. [15] is digitized, we can convert the  
 190 data to the relaxation of Young's modulus by a simple expression as:

$$191 \quad E(t) = \frac{\sigma}{\varepsilon(t)} \quad (2)$$

192 Having the time-dependent Young's modulus readily leads us to evaluate the time dependent  
 193 shear modulus. From that point, a nonlinear curve fitting tool can be employed to fit a curve in the  
 194 form of Prony series to the discrete data. By taking two exponential terms ( $N_M = 2$ ) in the Prony  
 195 series, a curve is fitted to the discrete shear modulus data using the nonlinear curve fitting tool of  
 196 MATLAB<sup>®</sup> [17].



197  
198

**Figure 4.** Prony series fit for the experimental shear modulus data.

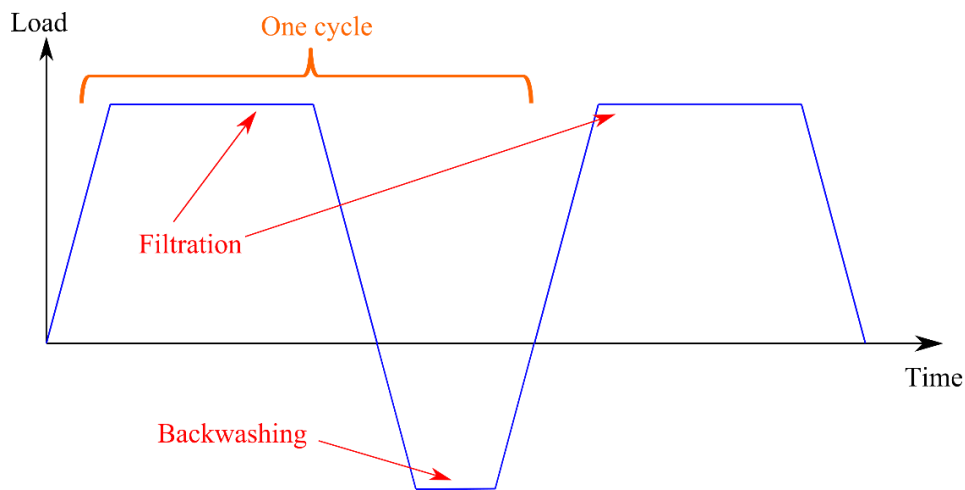
199 The correlation between the discrete data and the fitted curve can be observed in Figure 4. The  
 200 mathematical expression for the fitted curve is given as:

$$201 \quad G(t) = 5.228 + 8.758 \times e^{(-t/0.906)} + 31.92 \times e^{(-t/0.103)}. \quad (3)$$

202 The parameters in Eq. (3) should be properly introduced to a FE code for the viscoelastic simulation.

## 203 2.2. Mechanical Fatigue Life Calculations

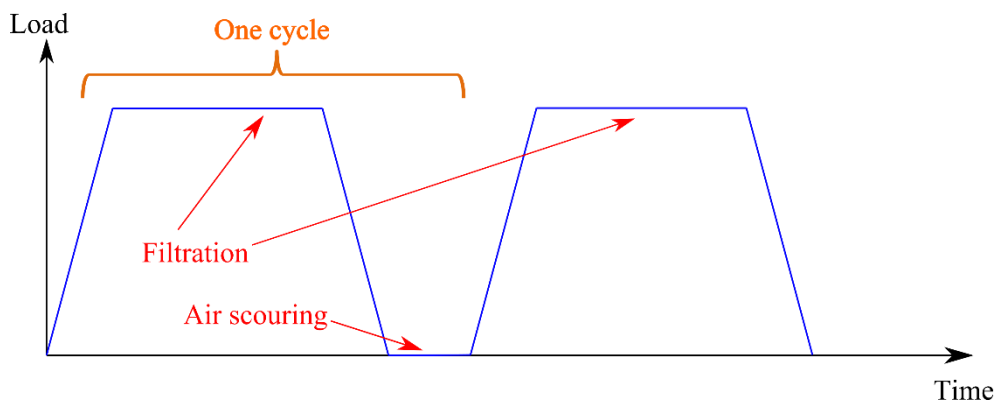
204 The fatigue simulations aim to provide life predictions of the membranes under variable  
 205 mechanical loads. The influence of the wear and corrosion of the membrane material are currently  
 206 not taken into account. The loading procedure and one load cycle definition for the cases with and  
 207 without backwashing implementation are given in Figures 5 and 6, respectively.



208

209

**Figure 5.** Loading procedure for filtration + backwashing cycle.



210

211

**Figure 6.** Loading procedure for filtration + air scouring cycle.

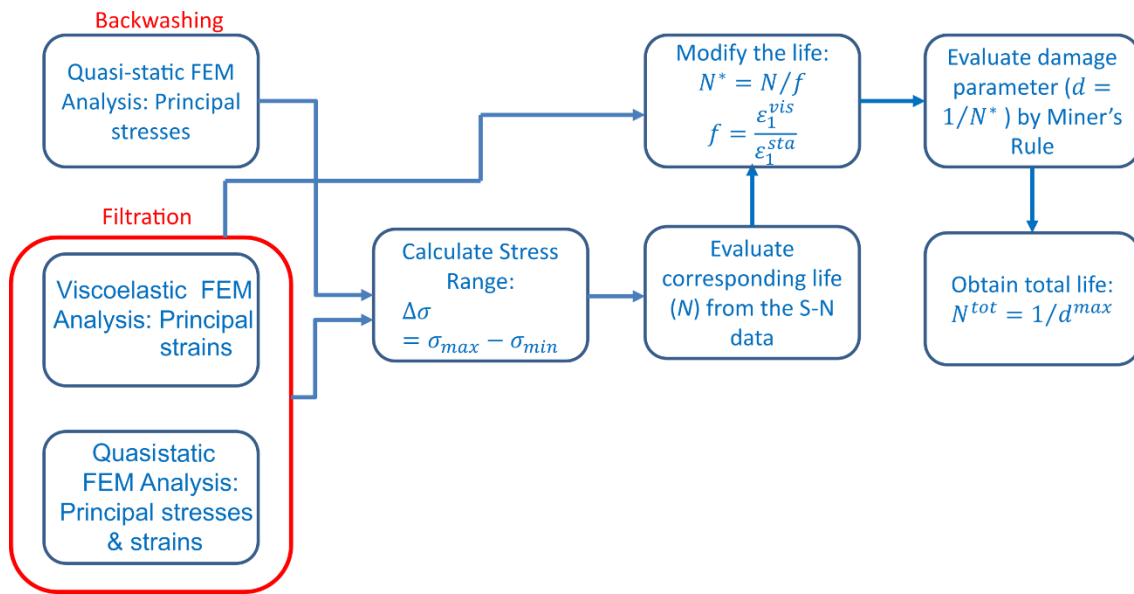
212 The duration of filtration is assumed as 2 hours, while the duration of the backwashing and the  
 213 air scouring is relatively short, i.e., 5 minutes. In this regard, the viscous effects are omitted for the  
 214 backwashing process.

215 Since it is known that the backwashing process may compromise the structural integrity of flat

216 sheet membranes, membrane fouling is usually controlled by membrane relaxation + air scouring. In  
 217 this process, it is assumed that the membrane sheet is unloaded and the air scouring does not generate  
 218 any significant stress on the membrane. The duration of membrane relaxation + air scouring is also  
 219 taken as 5 minutes.

### 220 2.2.1. Fatigue life calculation procedure

221 We employ a simplified fatigue life prediction method, which takes into account the viscous  
 222 deformation effects for filtration indirectly. The flowchart of fatigue life calculation procedure is  
 223 presented in Figure 7.



224

225 **Figure 7.** Fatigue life calculation procedure for the membrane sheets.

226 The process shown in Figure 7 is described as follows. First, we perform quasi-static analyses  
 227 for the filtration process. Then, the viscoelastic analysis should be performed for predicting the  
 228 long-term deformation of the membranes under filtration transmembrane pressure. Since the duration  
 229 of backwashing is much shorter than the filtration, we can omit the long-term effects for  
 230 backwashing. Then, only quasi-static analyses are performed for the membranes under backwashing  
 231 pressure.

232 We will extract maximum principal stresses and strains from the FE simulations. The stress  
 233 range will be calculated by the principal stresses from the quasi-static analyses of filtration and  
 234 backwashing. Once the stress range is calculated, the corresponding life from the S-N data can be  
 235 obtained. Then, this life should be modified for the long-term effects. A factoring coefficient is  
 236 employed for the modification purposes, which is the ratio of long-term 1<sup>st</sup> principal strain to the 1<sup>st</sup>  
 237 principal strain from the quasi-static analyses for filtration. Afterwards, fatigue damage parameter for  
 238 each cycle is obtained by Miner's sum. Finally, the total number of cycles for the fatigue life of the  
 239 membrane is obtained by relating it to the maximum damage parameter.

### 240 2.2.2. Miner's rule



241 The accumulation of the fatigue damage is obtained by the Miner's rule. Therefore, this method  
 242 is briefly touched here. The total damage on a particular location can be expressed as:

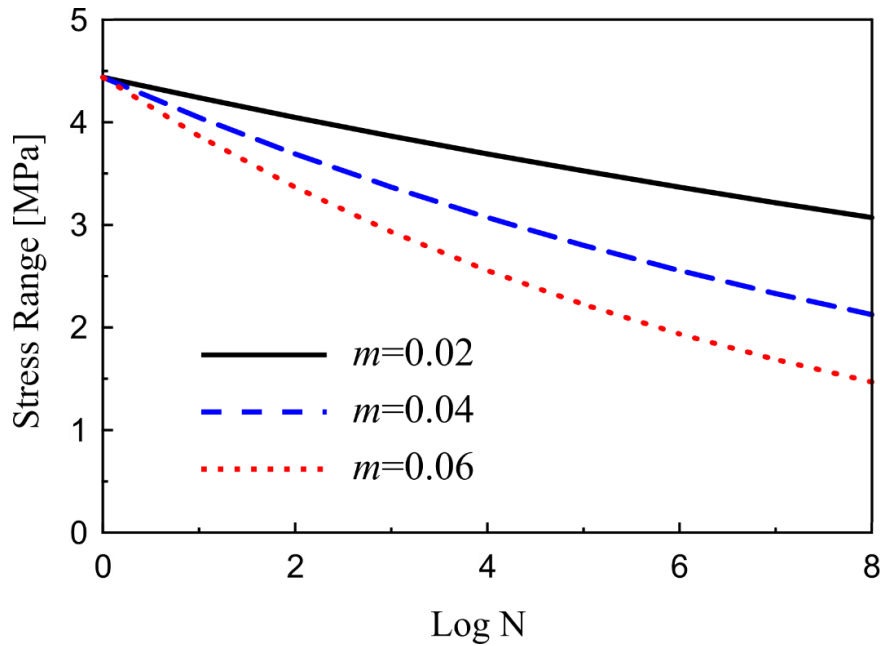
$$243 \quad D = \sum_i^k \frac{n_i}{N_i} \quad (4)$$

244 In Eq. (4),  $D$  represents the total damage at a certain location. The number of loading cycles at that  
 245 location for a certain stress range is denoted as  $n$ , while  $N$  is the corresponding total fatigue life at the  
 246 given stress range obtained by the S-N data at hand. The total number of stress range blocks are  
 247 represented by  $k$ . If the accumulated damage value,  $D$  becomes equal to 1.0 at any point in the  
 248 membrane sheet, it is assumed that the membrane fails due to the fatigue damage accumulation.

249 It is also important to note that the frequency of loading is neglected as it is too small because of  
 250 the longer filtration periods. Furthermore, the mean stress correction is not considered either due to  
 251 the lack of relevant data.

### 252 2.2.3. Fatigue properties

253 We aim to carry out fatigue life predictions based on the stress results obtained from the  
 254 quasi-static FE simulations. Moreover, we will not consider any pre-existing damage/crack on the  
 255 membrane sheets. In this regard, the fatigue life predictions are to be undertaken based on suitable  
 256 S-N relations. To the best of authors' knowledge, the available material fatigue data on PVDF  
 257 membrane materials are limited. Tng [18] presented some useful fatigue results for the hollow fibre  
 258 membranes under cyclic tensile loading. In addition to that, Solvay [19] published a design and  
 259 processing guide for PVDFs. When we digitize the S-N curve in [19], we have noticed that the  
 260 coefficient  $C$ , in the  $S = C \times N^{-m}$  form of expression, is slightly higher than the yield stress of the  
 261 considered material. The slope coefficient is  $m = 0.02$ . By invoking this similarity between the  
 262 coefficient  $C$  and the yield strength of the material, we assume a series of S-N curves for the PVDF  
 263 membrane sheet material in the present work. The form of the S-N relation is taken as  $S = C \times N^{-m}$ .  
 264 The parameter  $C$  is utilized as slightly higher than the yield strength of the material as  $C = 4.438$ ,  
 265 and the inverse slope coefficients are varied as  $m = 0.02, 0.04$  and  $0.06$  in the forthcoming  
 266 fatigue calculations. The comparison of the S-N curves for varying  $m$  values but the same  
 267 intersection point ( $C$  coefficient) with the vertical axis is provided in Figure 8.



268  
269 **Figure 8.** Comparison for S-N curves for varying  $m$  values.

270 It must be noted that the present S-N curve parameters are for the pristine material without any  
 271 long-term corrosion and environmental effects. The S-N data for the membrane materials under  
 272 corrosive environments have not been published in the open literature yet to the best of authors'  
 273 knowledge. However, the present fatigue life prediction procedure can be effectively adopted for the  
 274 membranes under corrosive environments as long as the proper S-N curves representing the  
 275 corrosion effects are adopted.

### 276 2.3. Test Scenarios

277 In this section, we summarize all the parameters and test cases for the proposed fatigue life  
 278 prediction and mechanical analysis procedures.

279 A single membrane sheet size is adopted in the present work as  $L \times W \times t_m = 500 \times 500 \times$   
 280  $2.0 \text{ mm}$ . For the same size of the membrane, the spacer configurations are adjusted as  $10 \times 10$   
 281 and  $20 \times 20$ . The change of the spacer configuration will impact the support conditions of the  
 282 membrane sheet under the filtration process, while the load and support condition will remain same  
 283 in the backwashing process for both spacer configurations.

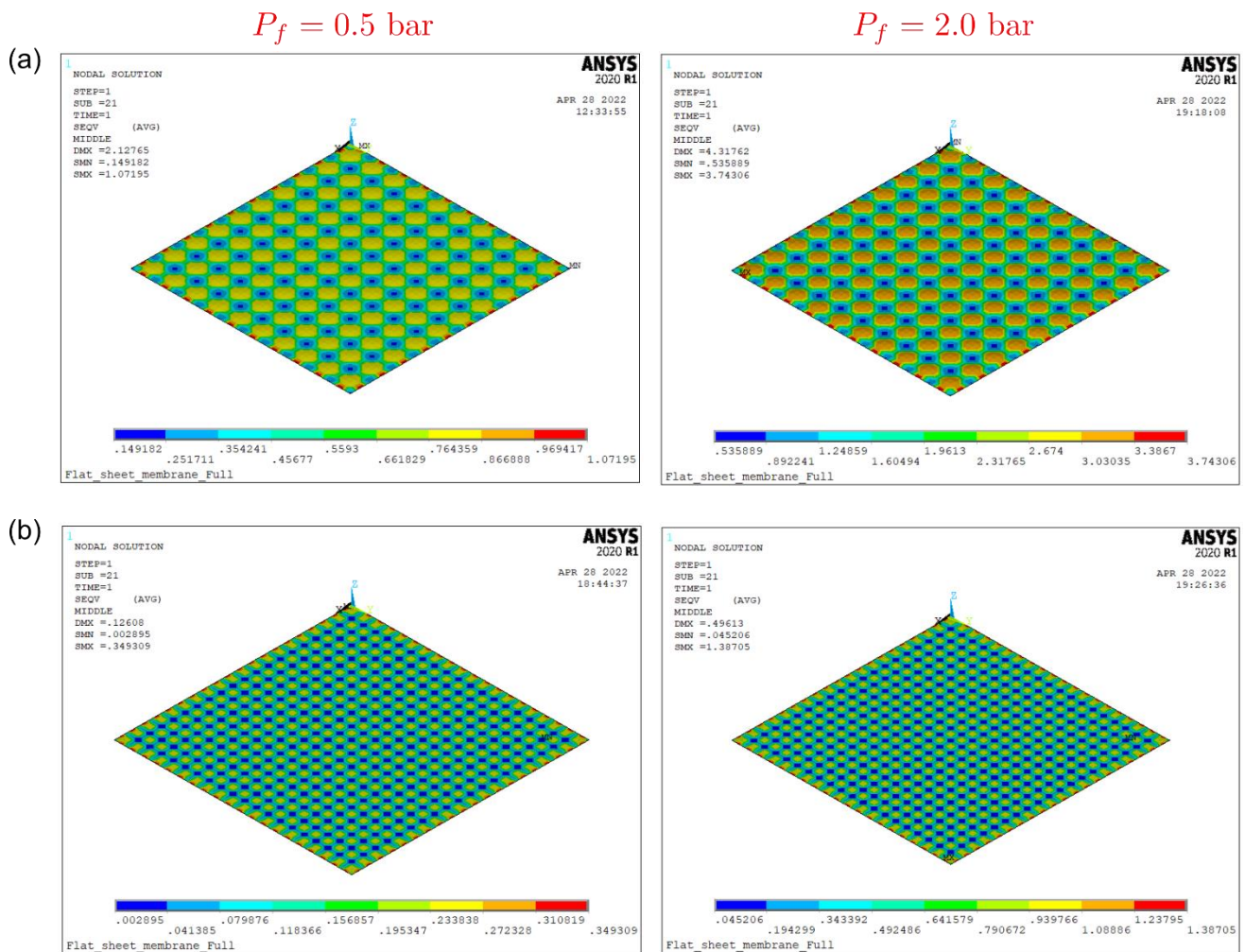
284 The vacuum filtration pressures are taken as:  $P_f = 0.5, 1.0, 1.5$  and  $2.0 \text{ bar}$ . These filtration  
 285 pressures are applied as uniform surface pressures on the membrane sheets. Since flat sheet  
 286 membranes are usually vulnerable to backwashing [20], we consider two different backwashing  
 287 conditions: (i) 2 hours of filtration without backwashing, (ii) 2 hours of filtration with a gentle  
 288 backwashing. The backwashing duration is practically several minutes. In the latter case, the  
 289 backwashing pressure is set as  $P_b = 0.1 \text{ bar}$ . In the first case, the fouling is to be controlled by the  
 290 membrane relaxation and air scouring after filtration. At this point, it is assumed that the load  
 291 variations acting on the membrane sheet due to the air scouring are insignificant and do not make  
 292 any change in the loading condition for fatigue life prediction procedure.

293 As described in the material modelling section, we will vary the slope coefficient,  $m$ , in the  
 294 fatigue life estimations for each loading configuration.

### 295 3. Results and Discussion

#### 296 3.1. Quasi-static FE Analyses

297 The first step in the mechanical durability assessment of flat sheet water treatment membranes is  
 298 the evaluation of stresses-strains and displacements under the static loading conditions. The results  
 299 will reveal useful information by an immediate check if the membrane sheets fail under the given  
 300 loads. More importantly, the stress results from these analyses will comprise the basis for the fatigue  
 301 life predictions.



302

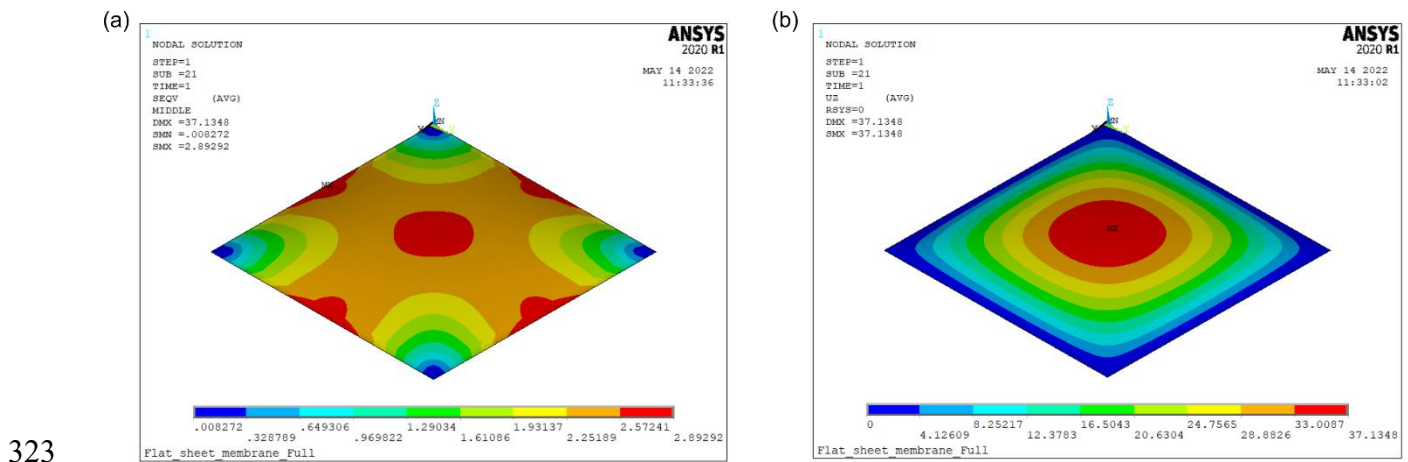
303 **Figure 9.** Equivalent (Von Mises) stress distribution [MPa]: (a)  $10 \times 10$  configuration, (b)  
 304  $20 \times 20$  configuration.

305 The equivalent stress distributions for  $P_f = 0.5$  and  $2.0 \text{ bar}$  are given in Figure 9. The results  
 306 for  $P_f = 1.0$  and  $1.5 \text{ bar}$  will fall in between the results presented in this figure; we therefore have  
 307 not given the stress results for these cases in Figure 9 to save the space. However, we have provided

308 the maximum values of the equivalent and principal stresses in Figure 11 for all pressures.

309 The stress distributions in Figure 9 apparently demonstrate the spacer configurations' effects.  
 310 Maximum equivalent stresses take place along the framing edge, which is the expected situation. In  
 311 the quasi-static analyses, the membrane is assumed to be intact; however, the stress distributions on  
 312 the membrane materials may show different patterns depending on degradation and localized damage  
 313 of the material in the long-term use.

314 The equivalent stress distribution and the displacement component normal to the membrane  
 315 surface for the backwashing condition are given in Figure 10. In all loading and spacer  
 316 configurations, the membrane sheet deforms below its elastic limits. One should pay attention to the  
 317 deformation of the membrane in the backwashing condition. Under the considered backwashing  
 318 pressure,  $P_b = 0.1 \text{ bar}$ , the maximum normal displacement is around 37 mm, which is far above the  
 319 membrane thickness. This large deformation also suggests that the pressure load is compensated by  
 320 the in-plane forces; the influence of the bending deformations is small. Excessive deformation may  
 321 cause the decline of permeate water quality in the long-term usage of the membranes. This issue will  
 322 be discussed quantitatively in the next section.



324 **Figure 10.** Backwashing results: (a) equivalent (Von Mises) stress distribution [MPa], (b)  
 325 displacement component normal to the membrane surface [mm].

326 The maximum values of the equivalent and the first principal stresses are given in Figure 11. The  
 327 maximum values of the equivalent stress and the 1<sup>st</sup> principal stresses are mostly similar; however,  
 328 the 1<sup>st</sup> principal stress values slightly exceed the equivalent stress values in the case of backwashing.  
 329

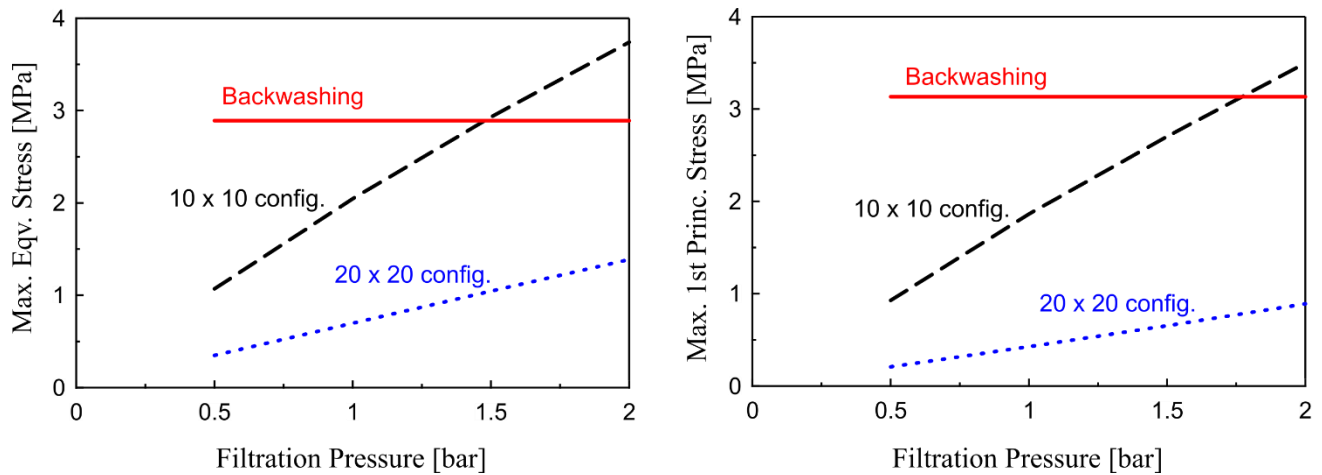


**Figure 11.** Maximum values of the main stress components.

The maximum values of the 1<sup>st</sup> principal stress values also suggest that the fatigue failure will likely to be controlled by the stresses occurring during the backwashing for the small and average filtration pressures, i.e.,  $P_f < 1.5 \text{ bar}$ .

At this point, it can be inferred that the membrane lives will be mainly characterized by the backwashing application for finer spacer configurations. If this is the case, allocating more spacers will not improve the overall fatigue life of the membrane.

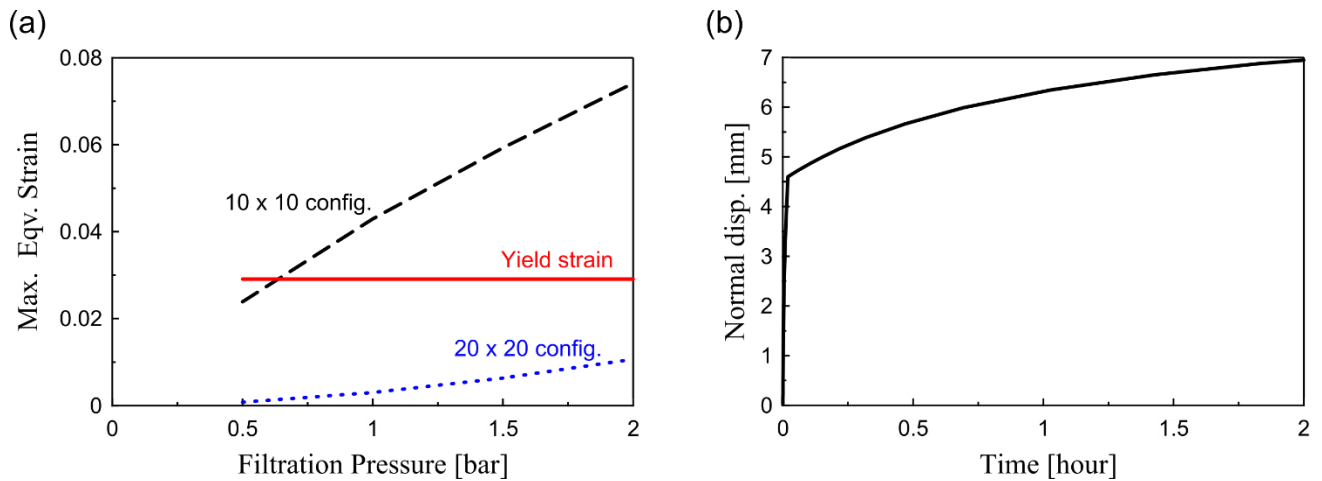
### 3.2. Viscoelastic Analyses

The response of the membrane sheets under the assumption of quasi-static loading has been examined in the previous section. Despite the results of the quasi-static analyses are meaningful for the assessment of the structural integrity of the viscoelastic membranes, they may not be adequate alone. It is therefore considered that the deformation of the membrane sheets under the long-term filtration pressure should be characterized.

The findings from the viscoelastic analyses could be utilized for the assessment of the permeate water quality as well as improvement of the fatigue life predictions. As described in the material modelling section, we will enforce the viscoelastic properties by means of the Prony series coefficient in ANSYS FE package [16].

A viscoelastic analysis is essentially a transient dynamic analysis without the inertia effects [21]. We therefore follow the procedure recommended in [21]. The simulation time is equal to the filtration duration, i.e.,  $t_{\text{sim}} = 2 \text{ hours}$ . The time increment size is set as variable based on the convergence rate of the FE simulation. The loading scheme is the one defined by Figure 3 (b) in Section 2.1.1. The load is gradually increased up to the desired level in a short period to avoid the numerical instabilities causes by the sudden implementation of whole load in a single step.

Since the stresses acting on the membrane sheet remain more or less the same during the viscoelastic simulations, we will focus on the displacement and strain values to assess the possible decline of the permeate water quality and the compromise of the structural integrity due to the excessive deformation.



358

359 **Figure 12.** Viscoelastic analyses results after 2 hours: (a) Maximum equivalent strain values, (b)  
 360 History of displacement component normal to membrane surface for  $10 \times 10$  configuration under  
 361  $P_f = 2.0$  bar.

362 Figure 12 (a) indicates that the maximum values of the equivalent strains for the  $10 \times 10$   
 363 spacer configurations exceed the yield strain of the membrane material at almost all filtration  
 364 pressure cases. We may infer that the nominal pore sizes for these cases may increase substantially,  
 365 which in turn the decline of the permeate water quality might occur. On the other hand, one can  
 366 readily see that the strain values for the  $20 \times 20$  spacer configurations remain below the yield  
 367 strain of the membrane material, which is the ideal situation for ensuring both the structural integrity  
 368 and permeate water quality.

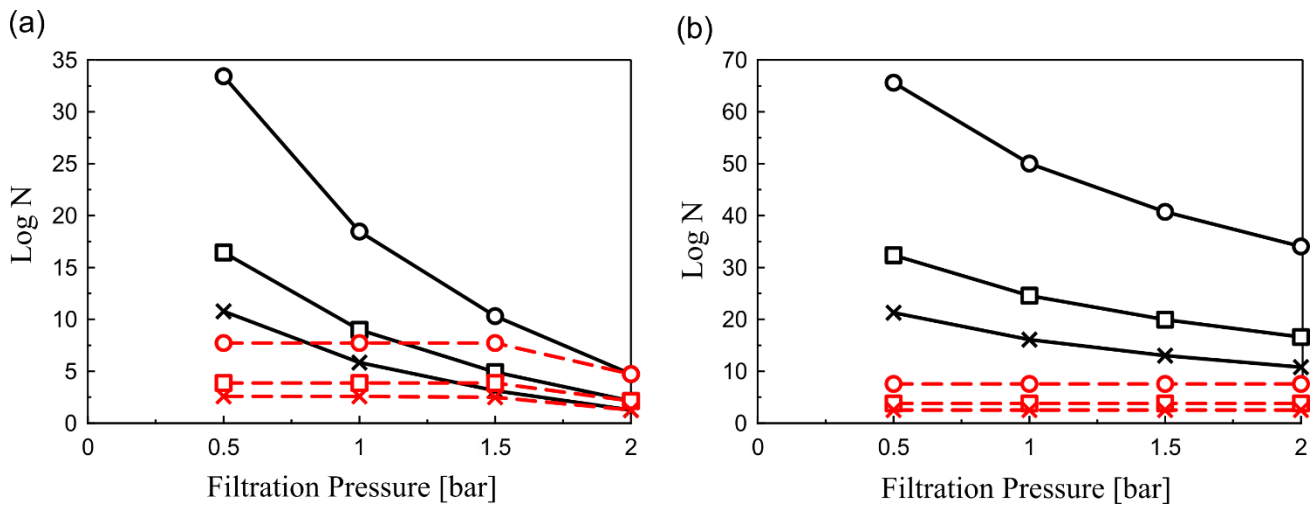
369 The displacement history of the membrane sheet for  $10 \times 10$  configuration under the highest  
 370 filtration pressure is given in Figure 12 (b). This figure apparently shows the viscous effects as the  
 371 displacements increase continuously by the time. The maximum value of the normal displacements  
 372 obtained by the quasi-static analyses in Section 3.1 is 4.32 mm, which is consistent with the  
 373 displacement value for  $t \cong 0$  in the viscoelastic analysis. When the simulation ends, the maximum  
 374 value of the displacement becomes almost 7 mm. A similar trend can be seen for the strain  
 375 components by the viscoelastic analyses.

376 Considering the increase of the displacements/strains under viscous effects, we will propose an  
 377 approach to account for viscous deformation effects indirectly in the fatigue life predictions.

### 378 3.3. Fatigue Life Predictions

379 The procedure described in the previous section and the FE stress-strain results are utilized for  
 380 the membrane mechanical life predictions. The fatigue life calculations are not performed only for  
 381 the designated stress hot spots, but also they are performed for all the FE nodal points to gather  
 382 damage distribution on the membranes.

383 The estimated mechanical fatigue lives (cycles) for the membrane sheets with and without  
 384 backwashing conditions are presented in Figure 13. The without backwashing cases are  
 385 demonstrated by solid black lines in Figure , while the fatigue lives for the filtration + backwashing  
 386 cases are illustrated by the dashed red lines. The different marker types stand for the filtration  
 387 pressure values. The circle “ $\circ$ ” marker is to represent  $m=0.02$ . The other inverse slope coefficients,  
 388  $m=0.04$  and  $0.06$  are denoted by square “ $\square$ ” and cross “ $\times$ ” markers, respectively.



389

390 **Figure 13.** Fatigue life predictions: (a)  $10 \times 10$  configuration, (b)  $20 \times 20$  configuration.

391 Due to the large number of cycles in some cases, the fatigue lives are presented in the  
 392 logarithmic scale in Figure 13. The fatigue cycles are then converted to *months* and presented in  
 393 Tables 1 and 2. The conversion is performed by assuming each cycle, filtration + air scouring or  
 394 filtration + backwashing, is about 125 minutes.

395

396 **Table 1.** Estimated mechanical fatigue lives [*month*] for flat sheet membranes with  $10 \times 10$   
 397 configuration.

| $P_f$ [bar] | $m = 0.02$ |             | $m = 0.04$ |             | $m = 0.06$ |             |
|-------------|------------|-------------|------------|-------------|------------|-------------|
|             | Backwash   | No Backwash | Backwash   | No Backwash | Backwash   | No Backwash |
| 0.5         | 1.497E+5   | 7.565E+30   | 20.67      | 7.855E+13   | 1.07       | 1.714E+8    |
| 1.0         | 1.497E+5   | 8.169E+15   | 20.67      | 2.796E+6    | 1.07       | 1.942E+3    |
| 1.5         | 1.495E+5   | 8.823E+7    | 20.67      | 239.56      | 0.89       | 3.84        |
| 2.0         | 151.06     | 151.06      | 0.39       | 0.39        | 0.05       | 0.05        |

398

399 The fatigue life predictions for  $10 \times 10$  spacer configuration are given in Table 1. As it is  
 400 presented in Table 1, the backwashing operation reduces the fatigue lives dramatically. It is because  
 401 of the fact that the outwards deformation of the membrane sheet under backwashing is not  
 402 constrained by the spacers. The variation of the inverse slope parameter,  $m$ , of the fatigue data  
 403 impacts the estimated fatigue lives. At this point, it must be noted that the material parameters have  
 404 the paramount impact on the estimated fatigue lives, and their accurate evaluation is crucial.

405 It is apparent that the fatigue lives of membranes become almost infinite in case of low filtration  
 406 pressures without backwashing. For example, the minimum fatigue life of the membrane with  
 407  $10 \times 10$  spacer configuration under  $P_f = 0.5$  bar is higher than  $10^{10}$  filtration cycles (1.714E+8  
 408 *months*). This is partly because the environmental effects are not considered in the present work due  
 409 to the lack of test data for the material under corrosive environments. It can be expected that fatigue  
 410 life of the membrane will be lower than such big number in the real applications. On the other hand,

411 it can be inferred that the fatigue failure of the membranes will be dominated by the stress cycles  
 412 rather than the corrosion under higher filtration pressures, e.g., the fatigue life of membranes  
 413 becomes a few hundred filtration cycles, i.e., less than a month for  $P_f = 2.0 \text{ bar}$ . In this case, it is  
 414 expected that the long-term corrosion effects will be negligible.

415 The fatigue life predictions for the  $20 \times 20$  spacer configuration cases are presented in Table  
 416 2. The most evident observation from the table is that almost infinite life predictions for the  
 417 membranes without backwashing cases. It may seem to be unrealistic; however, this outcome enables  
 418 us to infer that the membrane will not fail due to the mechanical fatigue, but the main cause of the  
 419 membrane failure would probably be the chemical erosion/wear of the membrane material.

420 **Table 2.** Estimated mechanical fatigue lives [*month*] for flat sheet membranes with  $20 \times 20$   
 421 configuration.

| $P_f$ [bar] | $m = 0.02$ |             | $m = 0.04$ |             | $m = 0.06$ |             |
|-------------|------------|-------------|------------|-------------|------------|-------------|
|             | Backwash   | No Backwash | Backwash   | No Backwash | Backwash   | No Backwash |
| 0.5         | 1.056E+5   | 1.185E+63   | 17.36      | 6.610E+29   | 0.95       | 5.441E+18   |
| 1.0         | 1.056E+5   | 2.976E+47   | 17.36      | 1.065E+22   | 0.95       | 3.508E+13   |
| 1.5         | 1.056E+5   | 1.526E+38   | 17.36      | 2.484E+17   | 0.95       | 2.922E+10   |
| 2.0         | 1.056E+5   | 3.117E+31   | 17.36      | 1.144E+14   | 0.95       | 1.764E+8    |

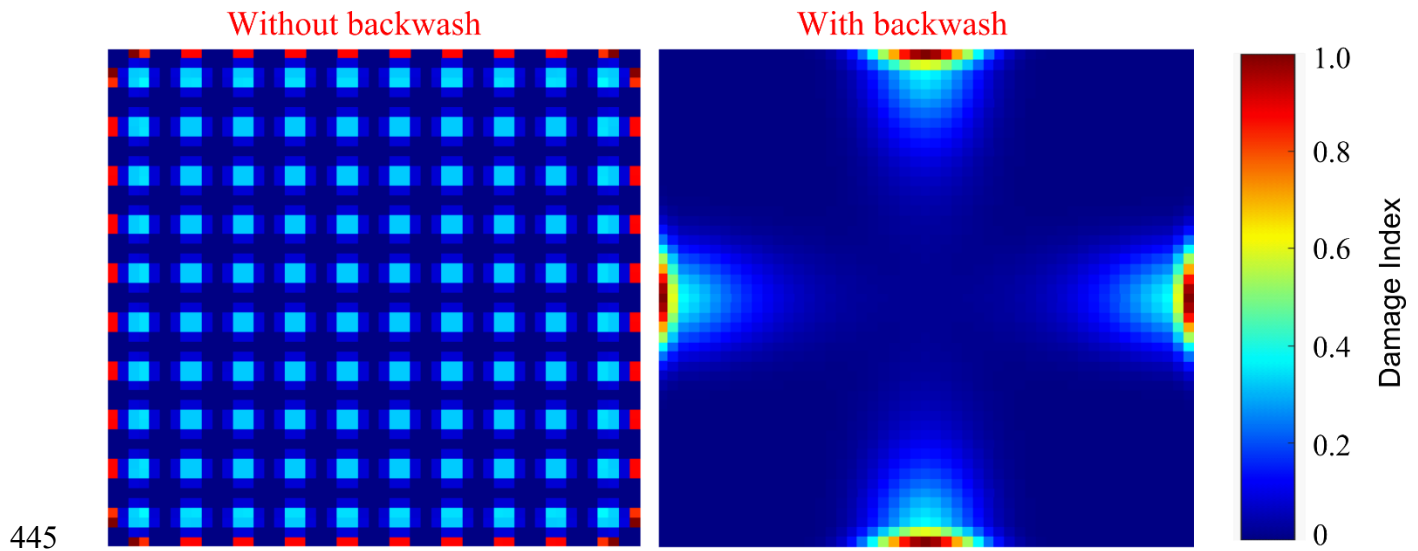
422 The impact of the material parameter  $m$  is obvious again. If there is no backwashing  
 423 implementation, the fatigue lives of the membranes become infinite even for the largest material  
 424 parameter considered ( $m = 0.06$ ). This circumstance suggests that the other material parameter  $C$  is  
 425 also a significant factor impacting the membrane lives.  
 426

427 Since there is no available fatigue data for the considered material under corrosive  
 428 environments, we have not been able to conduct fatigue simulations for the degraded membrane  
 429 materials. The main material parameter that will be affected by the corrosive environment is  $C$ ,  
 430 which will be lower than the present value ( $C = 4.438$  for intact material) in case of eroded  
 431 membrane materials; however, the inverse slope of the S-N curve ( $m$ ) for this material can be  
 432 expected to be in the presently considered range.

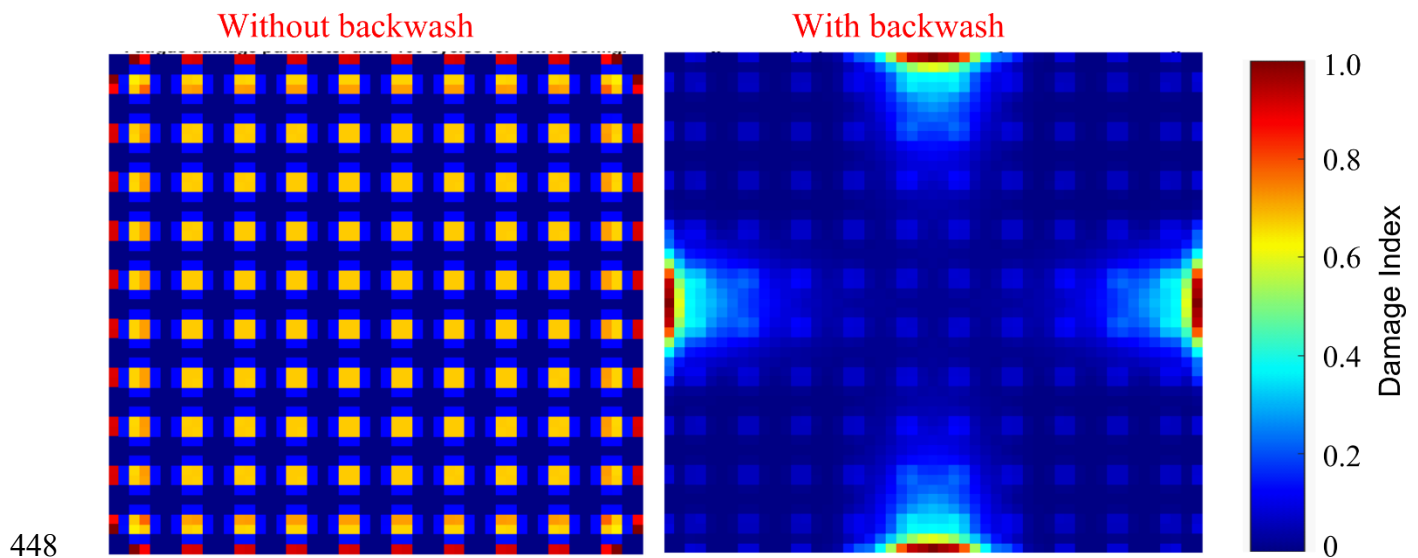
433 In addition to the discussions above, the following observations can be articulated. If the  
 434 filtration pressure is lower with backwashing, i.e.,  $P_f < 1.5 \text{ bar}$ , the fatigue lives become  
 435 unchanged for the variations of the filtration pressure. This is because of the fact that the  
 436 backwashing operation determines the total fatigue life, and the backwashing pressure is kept  
 437 constant in this study for all filtration pressure cases. As increase of the filtration pressure, the gap  
 438 between the fatigue lives for with and without backwashing cases disappears. For the highest  
 439 filtration pressure case, i.e.,  $P_f = 2.0 \text{ bar}$ , the estimated fatigue lives for with and without  
 440 backwashing cases are almost the same in  $10 \times 10$  configurations. This situation suggests that the  
 441 fatigue failure is dominated by the stresses under the filtration pressures.

442 Another evident observation is the gap between the fatigue lives for the membranes with  
 443 different spacer configurations when the backwashing is not implemented. The stresses become  
 444 significantly lower for the  $20 \times 20$  configuration, and so the longer fatigue lives.

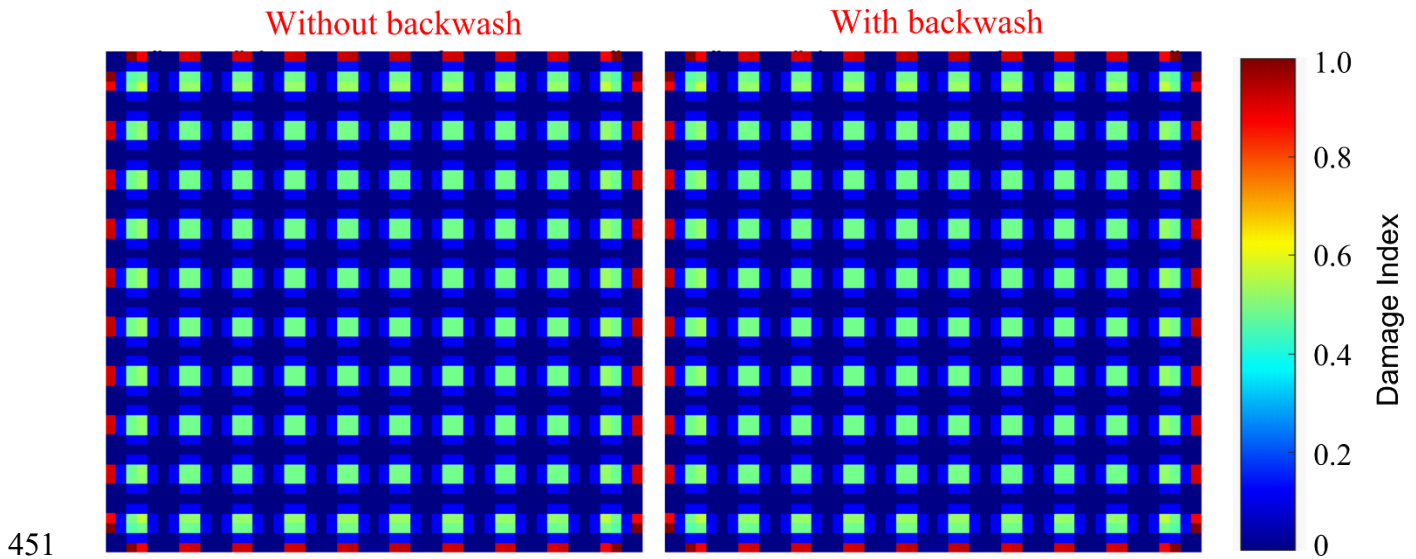




446 **Figure 14.** Accumulated damage patterns for  $10 \times 10$  configuration under filtration pressure,  
447  $P_f = 0.5 \text{ bar}$ .

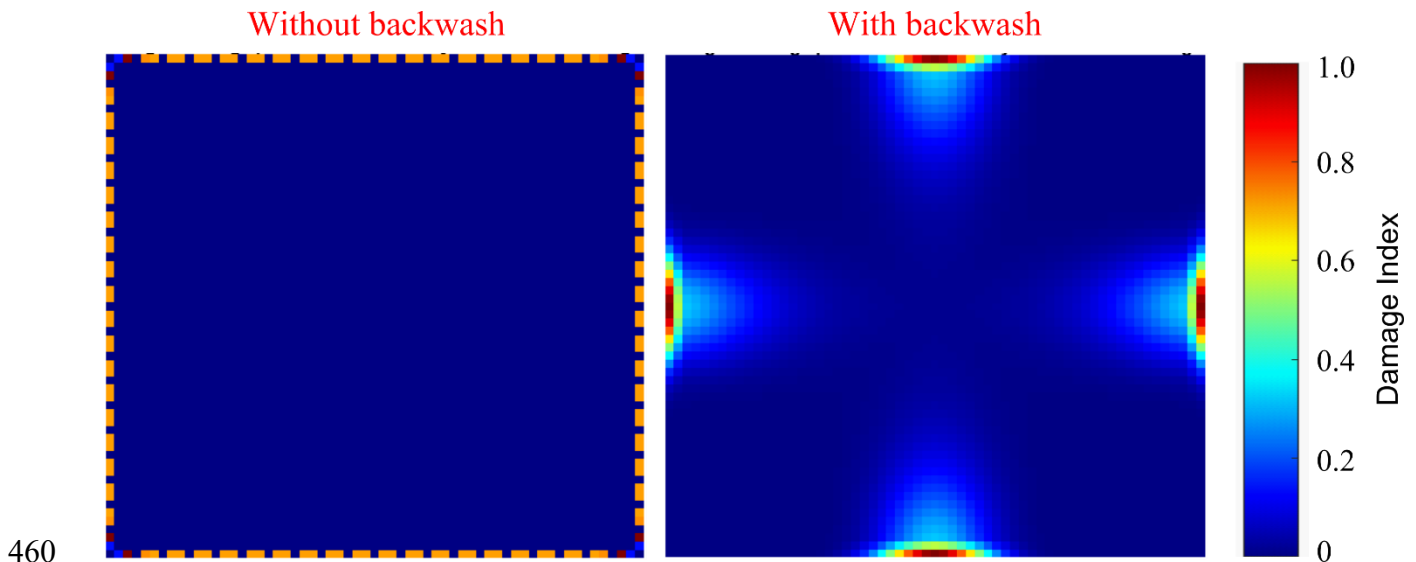


449 **Figure 15.** Accumulated damage patterns for  $10 \times 10$  configuration under filtration pressure,  
450  $P_f = 1.5 \text{ bar}$ .



452 **Figure 16.** Accumulated damage patterns for  $10 \times 10$  configuration under filtration pressure,  
 453  $P_f = 2.0 \text{ bar}$ .

454 The calculated fatigue damage patterns are independent of the inverse slope coefficients,  $m$ . Then,  
 455 the damage distributions for  $10 \times 10$  configurations for the selected filtration pressure cases are  
 456 given in Figures 14, 15 and 16 along with the colorbars representing the damage index throughout  
 457 the membrane sheets. All these figures suggest that the membrane failures occur along the framing  
 458 region due to the higher stresses. It is also obvious from these figures that the impact of filtration  
 459 pressure becomes visible on the damage patterns for the backwashing cases.



461 **Figure 17.** Accumulation of damage patterns for  $20 \times 20$  spacer configurations.

462 The accumulated damage patterns for  $20 \times 20$  configurations are almost the same regardless  
 463 of the considered filtration pressure values. If the backwashing is applied, the failure takes places on

464 the mid-edges of the sheet because of the backwashing deformations in all filtration cases, see Figure  
465 17. If the backwashing is not the case, the membrane lives becomes almost infinite, see Figure 13 (b);  
466 and the fatigue damage accumulates at the corner points, see Figure 17.

#### 467 **4. Conclusions**

468 A procedure for assessing the mechanical response and fatigue life of flat-sheet water treatment  
469 membranes has been presented. Then, the procedure has been demonstrated by an extensive study on  
470 the water treatment membranes. The proposed procedure is applicable for any thickness values of  
471 flat-sheet membranes. The main assumptions in the proposed methodology as well as the  
472 observations are summarized as follows.

473 The spacers are assumed to support the membranes under filtration, but the mechanical support  
474 of the spacers under backwashing is omitted as the flow direction is reverse and the membrane sheet  
475 deforms outwards.

476 Long-term viscoelastic analyses have revealed that the equivalent strains for  $10 \times 10$  spacer  
477 configurations exceed the yield strain of the membrane material in the most filtration cases. This  
478 situation is expected to compromise the permeate water quality.

479 We have proposed a simplified approach to account for the long-term deformation effects of the  
480 viscoelastic membranes in the mechanical fatigue life predictions. Fatigue failure damage of the  
481 membrane sheets are accumulated along the framing lines for all cases.

482 The membrane sheets with  $20 \times 20$  spacer configurations mostly remain mechanically safe as  
483 long as the backwashing is not implemented. In the  $20 \times 20$  spacer configurations, the membrane  
484 failure is dominated by the backwashing regardless of the filtration pressure. The assumption on the  
485 mechanical support of the spacers under backwashing pressure is a conservative approach, if a  
486 special configuration can be adopted to support membrane deformation under backwashing, the  
487 membrane lives can be improved significantly.

488 On the other hand, it is possible to observe the impact of filtration pressure on the fatigue  
489 damage accumulation for  $10 \times 10$  spacer configurations, particularly for  $P_f \geq 1.5 \text{ bar}$ .

490 In summary, the proposed procedure has been demonstrated through the case studies, and the  
491 main observation from the cases studies is that the membrane sheets become mechanically safe when  
492 the filtration pressure is  $P_f \leq 1.5 \text{ bar}$  and the backwashing is not implemented for the considered  
493 membrane sheet properties and spacer configurations. The proposed procedure can also be employed  
494 for the long-term fatigue life predictions under corrosive environment with the proper material data  
495 representing the actual conditions.

#### 496 **Acknowledgements**

497 This work was supported by an Institutional Links grant, ID 527426826, under the  
498 Egypt-Newton-Mosharafa Fund partnership. The grant is funded by the UK Department for Business,  
499 Energy and Industrial Strategy and Science, Technology and Innovation Funding Authority  
500 (STIFA) - project NO. 42717 (An Integrated Smart System of Ultrafiltration, Photocatalysis,  
501 Thermal Desalination for Wastewater Treatment) and delivered by the British Council.

#### 502 **Conflict of Interest**

503 The authors have no conflicts of interest to declare.

## 504 **References**

- 505 1. Judd S, Judd C, (2011) *The MBR Book*, Oxford: Butterworth-Heinemann.
- 506 2. Madaeni SS, Ghaemi N, Rajabi H (2015) Advances in polymeric membranes for water  
507 treatment,” In: *Advances in Membrane Technologies for Water Treatment*, Cambridge:  
508 Woodhead Publishing, 3-41.
- 509 3. Childress AE, Le-Clech P, Daugherty JL, et al. (2005) Mechanical analysis of hollow fiber  
510 membrane integrity in water reuse applications. *Desalination*, 180: 5-14.
- 511 4. Wang K, Abdalla AA, Khaleel MA, et al. (2017) Mechanical properties of water desalination  
512 and wastewater treatment membranes,” *Desalination*, 401: 190–205.
- 513 5. Ejaz Ahmed F, Lalia B, Hilal N, et al. (2014) Underwater superoleophobic cellulose/electrospun  
514 PVDF-HFP membranes for efficient oil/water separation. *Desalination*, 344: 48-54.
- 515 6. Hou D, Wang J, Sun X, et al. (2012) Preparation and properties of PVDF composite hollow  
516 fiber membranes for desalination through direct contact membrane distillation. *Journal of*  
517 *Membrane Science*, 405: 185–200.
- 518 7. Hong J, He Y (2012) Effects of nano sized zinc oxide on the performance of PVDF  
519 microfiltration membranes. *Desalination*, 302: 71-79.
- 520 8. Chartoff RP, Menczel JD, Dillman SH (2008) *Dynamic mechanical analysis (DMA), Thermal*  
521 *Analysis of Polymers*, John Wiley & Sons.
- 522 9. Chung TS, Qin JJ, Gu J (2000) Effect of shear rate within the spinneret on morphology,  
523 separation performance and mechanical properties of ultrafiltration polyethersulfone hollow  
524 fiber membranes. *Chemical Engineering Science*, 55: 1077-1091.
- 525 10. Lalia BS, Guillen-Burrieza E, Arafat HA, et al. (2013) Fabrication and characterization of  
526 polyvinylidene fluoride-co-hexafluoropropylene (PVDF-HFP) electrospun membranes for direct  
527 contact membrane distillation. *Journal of Membrane Science*, 428: 104-115.
- 528 11. Mackin TJ, Vernon PJ, Matthew RB (2004) Fatigue Testing of Polymer Membranes. *Polymer*  
529 *Composites*, 25(4): 442-450.
- 530 12. Hartinger M, Napiwotzki J, Schmid E.-M., et al. (2020) Influence of Spacer Design and Module  
531 Geometry on the Filtration Performance during Skim Milk Microfiltration with Flat Sheet and  
532 Spiral-Wound Membranes. *Membranes*, 10(4): 57.
- 533 13. Aerts PEM, Backwash Efficiency in IPC® Membrane modules for MBR,” 2019. Available from:  
534 <https://www.linkedin.com/pulse/backwash-efficiency-ipc-membrane-modules-mbr-peter-e-m-aerts/>  
535
- 536 14. ANSYS Mechanical APDL Basic Analysis Guide. ANSYS Inc., Canonsburg, PA , 2018.
- 537 15. Emori K, Miura T, Kishida H., et al. (2019) Creep deformation behavior of polymer materials  
538 with a 3D random pore structure: Experimental investigation and FEM modeling. *Polymer*  
539 *Testing*, 80: 106097.
- 540 16. ANSYS Mechanical APDL Material Reference. ANSYS Inc., Canonsburg, PA.
- 541 17. MATLAB, Curve Fitting Toolbox. Mathworks, 2022 Available from:  
542 <https://uk.mathworks.com/products/curvefitting.html>.
- 543 18. Tng KH (2018) *Mechanical Failure in Potable Reuse Plants: Component and System Reliability*  
544 *Considerations*. PhD Thesis, University of New South Wales, Sydney.
- 545 19. *Solef PVDF Design & Processing Guide*. Solvay.

- 546 20. Fane AG (2008) Submerged Membranes. In: *Advanced Membrane Technology and Applications*,  
547 New Jersey: John Wiley & Sons, 239-270.
- 548 21. ANSYS Mechanical APDL Structural Analysis Guide,” ANSYS Inc., Canonsburg, PA, 2018.